

Non-universality of front fluctuations for compact colonies of non-motile bacteria

Silvia N. Santalla,¹ Javier Rodríguez-Laguna,² José P. Abad,³ Irma Marín,³ María del Mar Espinosa,⁴ Javier Muñoz-García,⁵ Luis Vázquez,⁶ and Rodolfo Cuerno⁵

¹Physics Dept. & Grupo Interdisciplinar de Sistemas Complejos (GISC), Universidad Carlos III de Madrid, Leganés, Spain

²Fundamental Physics Dept., Universidad Nacional de Educación a Distancia (UNED), Madrid, Spain

³Departamento de Biología Molecular, Universidad Autónoma de Madrid (UAM), Cantoblanco, Madrid, Spain

⁴Hospital Universitario Puerta de Hierro, Madrid, Spain

⁵Mathematics Dept. & GISC, Universidad Carlos III de Madrid, Leganés, Spain

⁶Instituto de Ciencia de Materiales de Madrid (ICMM-CSIC), Madrid, Spain

Fronts of compact bacterial colonies growing on a Petri dish are considered a paradigmatic instance of non-equilibrium fluctuations in the celebrated Eden, or Kardar-Parisi-Zhang (KPZ), universality class. However, while the experimental scaling exponent values crucially do not agree with Eden-based predictions, the source of this disagreement has remained poorly understood. We have performed growth experiments with *E. coli* ATCC 25922 and *B. subtilis* 168 under conditions in which single bacteria motility is suppressed, leading to compact colony formation in the putative Eden regime. We put forward a continuum model whose comparison with numerical simulations indicates that the experimental scaling with non-Eden exponents is an effective non-universal behavior induced by the diffusive morphological instabilities that dominate the large-scale behavior. Hence, Eden/KPZ asymptotics are ruled out for this class of systems. Our conclusions agree with recent analytical results for alternative models which make closer contact with biological reaction-diffusion mechanisms.

Active matter —i.e., the emergent behavior of a large number of agents that can produce motion or mechanical forces at the expense of energy dissipation [1]— is recently proving itself as an extremely rich context for non-equilibrium phenomena. Active matter systems range from schools of fish or bird flocks, to vibrated granular rods or propelled nanoscale/colloidal particles, for all of which fluctuations play a conspicuous role in the collective dynamics [2].

Bacterial systems [3] provide further instances of active matter, from microswimmer suspensions in which individual cell motility plays a crucial role [4, 5] to bacterial colonies, in which it can be (strongly) hampered [6–8]. Actually, the fronts of bacterial colonies have long been considered as textbook examples [9–11] to illustrate how interactions among individuals lead to collective, highly-correlated spatio-temporal behavior. For experiments frequently done using *Bacillus subtilis* or *Escherichia coli*, this ranges from the formation of characteristic patterns —like diffusion-limited aggregation (DLA) fractals, concentric rings, or dense-branched morphologies— to the occurrence of disks or of compact, albeit rough, morphologies [7, 12–15], all of which are also found in other, non-living, systems.

The simplest situation in which individual bacterial motility is fully suppressed by a high agar concentration on the supporting Petri dish has received particular attention, as it paradigmatically demonstrates a change from DLA branches to compact, Eden-like, clusters, for an increasing nutrient concentration [8], akin to that found for many other DL growth systems [16]. This morphological transition has been recently shown to bear direct importance on the biological performance of the colony [17–19]. Thus, branches allow for spatial segregation of cell lines which respond differently with respect to the production of enzymes necessary for biofilm formation, enhancing the prevalence of cooperative cells. Biofilms are surface-attached communities hosting most liv-

ing bacteria in nature, of paramount importance to medicine and technology, from infections to energy harvesting [20, 21].

Furthermore, front fluctuations of Eden clusters [22] are known to be in the celebrated Kardar-Parisi-Zhang (KPZ) [23] universality class of kinetic roughening [10, 24, 25]. Sparked by breakthroughs on the exact solution of the KPZ equation and related growth models, that have been experimentally validated (for reviews, see e.g. [26–28]), this class is recently focusing an enormous attention. Indeed, it is being found to encompass the scaling behavior of many fluctuating 1D systems, like classical non-linear oscillators [29], stochastic hydrodynamics [30], quantum liquids [31], superfluids [32], or Fisher waves [33]. Remarkably, beyond critical exponents values, universal KPZ scaling also applies to the probability distribution—the Tracy-Widom distribution for the largest eigenvalue of Hermitian random matrices [26–28]— and the two-point correlation function [34, 35] of interface fluctuations.

Given the above, it is striking that, in the low motility case, the experimental values for the kinetic roughening exponents of compact Eden-like bacterial colonies *do not* coincide with the KPZ values [8, 13, 14]. Reconciling this fact with a putative Eden behavior requires invoking additional effects like e.g. quenched disorder [8], unexpectedly for a system which is quite successfully described by reaction-diffusion, continuum [36–39] or discrete [17, 40] models in which there is no source of quenched disorder.

In this Letter, we report colony growth experiments for *B. subtilis* 168 and *E. coli* ATCC 25922 under suppressed-motility conditions [15, 41]. We explain the non-KPZ kinetic roughening exponents that we indeed measure as effective scaling behavior induced by the diffusive instabilities that occur. This is achieved by comparing our data with simulations of a continuum model that we formulate, indicating that the experimental conditions keep the system within a DLA-dominated transient, for all accessible times. Moreover,

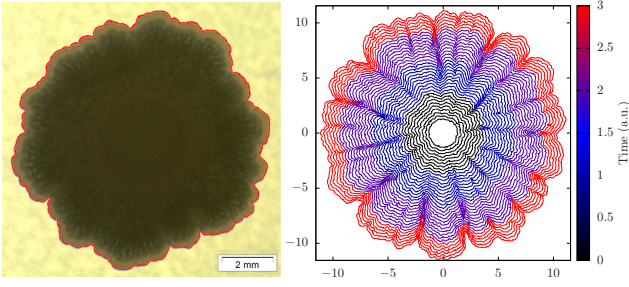


FIG. 1: Left: Sample experimental photograph of a *B. subtilis* colony (dark area), grown for a nutrient concentration of 20 g/l during 168 h. The red solid line shows the front position extracted as described in the SM [46]. Right: Interfaces provided by a numerical simulation of Eq. (1) for $A_0 = 0$, $A_1 = 0.1$, $A_S = 1$, $A_n = 0.1$ and a circular initial condition. The growth time for each profile can be read from the color bar on the right. Space and time units are arbitrary.

asymptotics are not in the KPZ universality class, so that Eden behavior is to be ruled out under suppressed-motility conditions. Analogous transient, non-universal behavior has been identified in other DL systems, like thin film growth by electrodeposition (ECD) or by chemical vapor deposition (CVD) [16, 42], or in coffee ring formation by evaporating colloidal suspensions [43–45].

We have grown colonies of *E. coli* and *B. subtilis* on Petri dishes as in [41], in the regime of a high agar concentration, i.e., low motility, for different concentrations of nutrients. Specifically, we have kept a constant agar concentration $C_a = 10$ g/l while considering different values of the nutrient concentration in the range $C_n = 10$ –20 g/l. This range of values is fully within the Eden-like region in morphological space [15, 41]. From the modeling point of view, these conditions correspond to a value for the non-dimensional thickness δ of the active layer—within the bacterial colony—where the nutrient concentration has non-negligible gradients [17, 37, 39, 40], which is large enough for the colony to look compact on the accessible space-time scales.

For inoculating Petri dishes, bacteria were grown overnight in nutritive liquid medium [5 g/l NaCl (Merck, Germany), 3 g/l meat extract (Merck, Germany), 10 g/l bacto-peptone (Laboratorios Conda, Spain)] and the OD600 was measured. Cells were pelleted at 12 krpm in a microcentrifuge, and resuspended to 0.5 OD600 in minimal medium without bacto-peptone [20 g/l NH_4Cl (Merck, Germany), 40 g/l KH_2PO_4 (Carlo Erba, Italy), 48 g/l Na_2HPO_4 (Merck, Germany), adjusted to pH 6.4 with HCl (Merck, Germany)]. Two replica Petri dishes were prepared following [41]: a 3 mm thick agar plate inoculated at the center with 1 μl of the cell suspension was incubated at 35 °C in a closed humid chamber for up to 33 days, leading to growth of quasi-two-dimensional colonies.

Pictures were taken at different incubation times using a digital camera (Olympus SC30, Japan; 3.3 Mp) coupled to a stereo microscope (Olympus SZX10), or a digital camera (Nikon D5000, Japan; 12.3 Mp) for large enough colonies. These photographs were treated as described in the Supple-

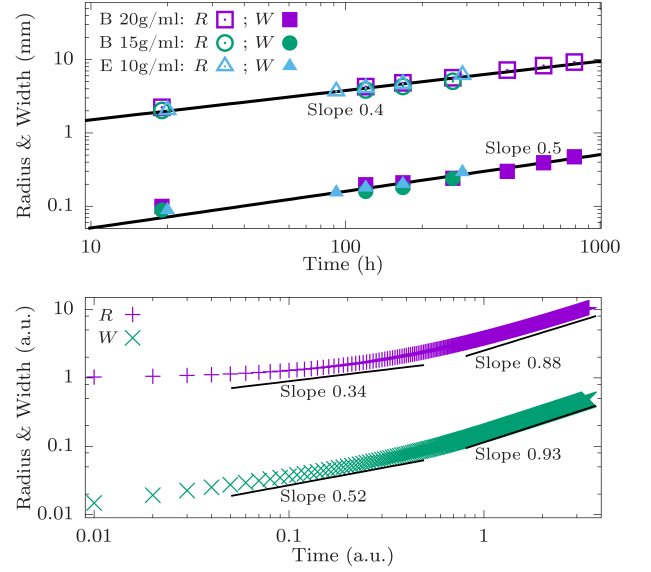


FIG. 2: Top panel: Log-log plot for the average radius R (upper sets of data) and roughness or surface width W (lower sets) vs growth time measured for several bacterial colonies. Space (time) units are mm (hours). *B. subtilis* (B) has been studied with a nutrient concentration of 15 g/l and 20 g/l. *E. coli* (E) has been studied with 10 g/l. Symbols are experimental data (error bars of the order of the symbol size, or smaller), while lines are fits to power laws, $R \sim t^n$ and $W \sim t^\beta$, with exponent values $n \approx 0.4$ and $\beta \approx 0.5$. Note the similarity in the power laws for different data. Bottom panel: Analogous of top panel, but for numerical simulations of Eq. (1) for parameters as in Fig. 1, averaged over 500 noise realizations. The lines represent power-laws $R \sim t^n$ and $W \sim t^\beta$ with different values of n and β for short and long times, as indicated. Units are arbitrary.

mental Material (SM) [46], to extract the position of the colony front at each growth time, see an example in Fig. 1. Note the compact form of the bacterial colony, which is delimited by a well-defined front that displays fluctuations around an average circular shape. The extracted front profile, which is a set of points on the plane, $\{x_i, y_i\}$, is used to obtain the radius R of the best fitting circle, using a minimization procedure that yields the center $(x_{\text{CM}}, y_{\text{CM}})$. Deviations from this circle provide the global roughness or surface width, W , see Eq. (2) in the SM [46].

Figure 2 shows the time evolution of the average radius and global roughness for our experimental colonies. Both behaviors can be fit by power laws $R(t) \sim t^n$ and $W(t) \sim t^\beta$, with $n \simeq 0.38$ –0.43 and $\beta \simeq 0.47$ –0.52, with quite similar values, independently of species and of nutrient concentration. Usually, for experimental circular interfaces that display Eden/KPZ fluctuations [43, 47]—conspicuously including (Vero) cell aggregates [48]—, the average front velocity is constant, hence the average front position increases linearly with time. At variance with this, the radial growth rate we measure is sublinear, i.e., $n < 1$. On the other hand, W follows power-law behavior with time as in standard kinetic roughening systems, with large β values, typically suggestive of uncorrelated, or possibly unstable growth [9–11]. Note

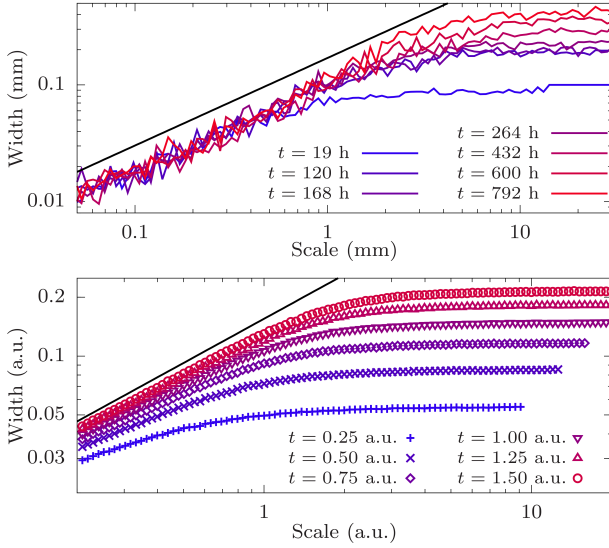


FIG. 3: Top: Morphology of the observed interfaces for *B. subtilis*, as described by the length-scale dependence of the roughness for different times. Bottom: Roughness dependence with length-scale as obtained from numerical simulations of Eq. (1) in the short-time regime of the right panel of Fig. 2. The solid lines correspond to $w(\ell) \sim \ell^{0.75}$ in both panels.

that, as reviewed in [8], to date no other experimental work on bacterial colony growth provides information on the time evolution of $R(t)$ or $W(t)$ under the present working conditions, in spite of the fact that universality classes are defined by at least two independent exponents [9–11], one of them related with time-dependent behavior.

In the case of *B. subtilis* we have also studied the geometrical properties of front fluctuations through the length-scale dependence of the roughness, $w(\ell)$, see Fig. 3. Namely, $w(\ell)$ is the mean-square deviation of the front positions to a fitting line extending a distance ℓ along the interface, see details in [49] and in the SM [46]. As seen in Fig. 3, there is an intermediate range of scales, approximately between 100 μm and 10 mm, within which a power-law dependence holds, $w(\ell) \sim \ell^\alpha$, for $\alpha \simeq 0.65\text{--}0.75$. Such a large value for the roughness exponent α coincides within error bars with those found earlier for similar bacterial colony experiments [8, 13, 14]. It is also very close to values measured in other DL systems, like 1D ECD [50, 51] or 2D thin films grown by CVD under low sticking conditions [52, 53], where such large α values are known to be non-universal [16, 42, 54] and to reflect the large surface slopes that ensue, due to diffusive instabilities.

In Fig. 4 we also show the correlation between the radial fluctuations of the interface as a function of the angular distance, $C(\Delta\theta) \equiv \langle (r(\theta) - R)(r(\theta + \Delta\theta) - R) \rangle$, in the case of *B. subtilis* for different times. Remarkably, the correlation vanishes approximately at the same angular distance for different times, consistent with branching of the front, which is a hallmark of the DL systems.

With hindsight from the study of kinetic roughening in diffusion-limited systems, and supported by more detailed

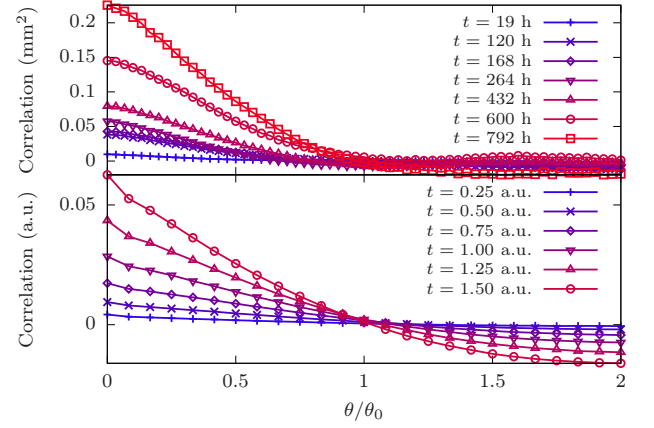


FIG. 4: Top panel: Autocorrelation function of radial fluctuations for *B. subtilis* as a function of angular distance, for different times. Correlation is measured in mm^2 . Bottom panel: Same observable for simulations of Eq. (1) with the parameters given in Fig. 1. Angles are rescaled by $\theta_0 = 30^\circ$ (12°) for experiments (simulations).

continuum models of bacterial colonies [37–39], we can actually account for our present experiments by an effective continuum model for the dynamics of the front position. Namely, we assume that the colony front is a closed simple curve that tends to minimize its length. Furthermore, we assume that the depth of the active layer δ [17, 37, 40] is sufficiently small that the evolution of the nutrient concentration field within the colony can be neglected, and merely assume that the nutrient diffusion currents from the outside reach bacteria which sit at local front protrusions preferentially, as compared with those at front troughs. Finally, nutrient transport and consumption, as well as cell division and relocation, are ultimately affected by stochastic fluctuations, which are expected to influence the local front velocity. The simplest dynamical model for the front that implements these assumptions reads

$$\partial_t \vec{r} = (A_0 + A_1 K(\vec{r}) + A_S \Theta_S(\vec{r}) + A_n \eta) \vec{n}, \quad (1)$$

where \vec{r} runs over the points of the interface and \vec{n} is the local exterior normal, $K(\vec{r})$ is the local extrinsic curvature, $\Theta_S(\vec{r})$ is the local aperture angle, and η is Gaussian, uncorrelated, space-time noise, and A_j are constants with A_0 describing the average velocity of a flat front. Equation (1) holds for a front with an arbitrary geometry and is not constrained by a small-slope approximation. Related models have been considered in DL growth, as for thin solid films [52, 54, 55] or combustion fronts [56, 57]. As shown there, the Θ_S term, which computes the local exposure angle to diffusive fluxes (see details at [46]), implements conveniently the non-local shadowing effects mentioned above, by which front cavities receive less nutrients and stagnate growth. Note, this does not imply the existence of quenched disorder, inexistent in Eq. (1).

Equation (1) is highly non-linear. We have simulated it numerically using an adaptive scheme which is similar to the one employed in [49, 58] for related models, see details in the SM [46]. Importantly, although the interface can have over-

hangs, it always remains a simple curve: self-intersections are removed and the largest component of the curve is retained. The evaluation of the shadowing angle is the most expensive part of the calculation, since it is a global quantity. The right panel of Fig. 1 shows the time evolution of an initially circular interface from simulations for a representative choice of parameter values. Once the interface perimeter becomes large enough, the shadowing instability sets in, leading to formation of “fingers” separated by relatively long “crevasses”. In spite of the assumed negligible value of δ , at all times the colony (the interior of the region bounded by the interface) remains a compact aggregate, with a boundary which shows fluctuations around an average circular shape. Note the strong similarity to the experimental profile on the left panel of Fig. 1.

We have studied quantitatively the dynamics of the front fluctuations described by Eq. (1). Figure 2 (bottom) shows the time dependence of the average radius and global roughness, as obtained in our simulations. For long enough times, both R and W grow almost linearly with time. However, shorter times correspond to a transient, within which both quantities increase much more slowly. One can fit their behavior to power laws, but the exponents become time-dependent. As the crossover time to the large-scale regime depends on equation parameters (hence, on experimental conditions), these exponents will also be parameter-dependent, hence non-universal. For the particular parameter choice and early-time region reflected in Fig. 2, the power-law behavior of $R(t)$ and $W(t)$ features exponents which are similar to those found in our experiments, $n = 0.34$ and $\beta = 0.52$, respectively. Finally, further support for our modeling comes from the behavior of the local roughness with length scale, as compared with the experimental result, see Fig. 3. Indeed, within the early-time regime, the model yields $w(\ell) \sim \ell^{0.75}$, very close to the experimental behavior. The autocorrelation functions provide further support for our claim: the bottom panel of Fig. 4 shows that the correlation angle stays constant both in the experiments and the simulations at this stage.

Comparison between our experimental results and numerical simulations suggests that the scaling properties seen in the former, as well as those reported in other, classical, experiments [13, 14], is preasymptotic behavior. Seemingly, parameter conditions in this system make the long-time regime hardly accessible; note that our longest experiments already reach up to 800 hours. Furthermore, our model indicates that, even if the long-time regime were accessible, it is not in the Eden/KPZ universality class; note e.g. the non-KPZ scaling behavior $W \sim t^{0.93}$ obtained for Eq. (1) at long times, see Fig. 2. Actually, a small-slope approximation of Eq. (1) leads to a non-local equation [16] whose asymptotics feature dimension-independent exponents $\alpha = \beta = 1$ [59]—recently measured in CVD growth under DL conditions [54]—, which are definitely non-KPZ and are expected to characterize Eq. (1) at long times. Note, for so-called super-rough interfaces with $\alpha \gtrsim 1$ [10, 60], local measurements through $w(\ell)$ or height correlation functions are known to underestimate the correct value of the roughness exponent [42].

To summarize, bacterial colonies in which individual motility is suppressed form compact aggregates whose front morphology is nevertheless dominated by diffusive instabilities. The scaling properties for which these systems have been considered paradigmatic are preasymptotic behavior, which is not in the Eden/KPZ universality class. There is no need to invoke quenched disorder effects to account for this discrepancy. Rather, the ensuing shadowing instability induces large front fluctuations with effective scaling behavior. The situation is similar to many other experimental growth systems [43, 50–53] in which transport-induced instabilities induce effective super-rough or other types of so-called anomalous scaling [10, 42, 60]. The analogy carries over to the extent that in some of these cases [43] the observed kinetic roughening has also been attributed to the so-called quenched KPZ (qKPZ) universality class, due to the accidental similarities in the numerical values of the scaling exponents [44, 45].

Very compact colonies with extremely flat fronts can be also found for nonmotile bacteria —e.g. in agent-based simulations [40]—, if the active layer thickness δ is sufficiently large. This may seem to question the prevalence of the diffusive instabilities which we are presently advocating for. However, continuum models [38, 39] analytically predict such flat front conditions to be a finite-size effect. Thus, (experimental) parameter conditions select a typical wavelength ℓ_0 for the diffusive instabilities, which is well defined for any value of δ . However, for the instability to actually set in, the correlation length along the front—initially a few cell sizes across—has to increase up to ℓ_0 . If this value is macroscopically large, the front may effectively be flat. For sufficiently (perhaps, exceedingly) long times, the instability will still occur.

We should also note that additional systems exist, which are closely related to the ones we study, and for which Eden/KPZ scaling does occur. For instance, bacterial colonies for which individual motility is non-negligible [14] yield a roughness exponent compatible with the 1D KPZ value. Also, aggregates of non-cancerous (Vero) or cancerous (HeLa) primate cells display unambiguous KPZ [48], and even qKPZ [61, 62], scaling, as is the case with fungal growth [63]. Experimentally, KPZ scaling also characterizes front fluctuations at frontiers between different genetic strains in range expansion of *E. coli* [64], although here deviations from Eden behavior can also occur [65, 66]. In general, individual cell motility seems to play a relevant role, to the extent that instabilities associated with nutrient transport can eventually be efficiently superseded. Indeed, the Eden model [22] will at any rate stand as the paradigmatic example for reaction-limited growth [9–11], in which nutrient transport is assumed to be infinitely fast and becomes irrelevant to front fluctuations.

We acknowledge fruitful conversations with G. Melaugh and K. A. Takeuchi. This work has been supported by the Spanish government (MINECO/AEI/FEDER/UE) through grants FIS2012-38866-C05-01, FIS2015-66020-C2-1-P, FIS2015-69167-C2-1-P, FIS2015-73337-JIN, and BIO2016-79618-R, and by Comunidad Autónoma de Madrid (Spain) Grant NANOAVANSENS S2013/MIT-3029.

-
- [1] S. Ramaswamy, *Ann. Rev. Condens. Matter Phys.* **1**, 323 (2010).
- [2] M. C. Marchetti, J. F. Joanny, S. Ramaswamy, T. B. Liverpool, J. Prost, M. Rao, and R. A. Simha, *Rev. Mod. Phys.* **85**, 1143 (2013).
- [3] E. Ben-Jacob, I. Cohen, and H. Levine, *Adv. Phys.* **49**, 395 (2000).
- [4] A. Sokolov, I. S. Aranson, J. O. Kessler, and R. E. Goldstein, *Phys. Rev. Lett.* **98**, 158102 (2007).
- [5] H. P. Zhang, A. Be'er, E.-L. Florin, and H. L. Swinney, *Proc. Natl. Acad. U.S.A.* **107**, 13626 (2010).
- [6] E. Ben-Jacob, I. Cohen, and D. L. Gutnick, *Ann. Rev. Microbiol.* **52**, 779 (1998).
- [7] M. Matsushita, F. Hiramatsu, N. Kobayashi, T. Ozawa, Y. Yamazaki, and T. Matsuyama, *Biofilms* **1**, 305 (2004).
- [8] J. A. Bonachela, C. D. Nadell, J. B. Xavier, and S. A. Levin, *J. Stat. Phys.* **144**, 303 (2011).
- [9] T. Vicsek, *Fractal growth phenomena* (World Scientific, Singapore, 1992).
- [10] A.-L. Barabási and H. E. Stanley, *Fractal concepts in surface growth* (Cambridge University Press, New York, 1995).
- [11] P. Meakin, *Fractals, scaling and growth far from equilibrium* (Cambridge University Press, Cambridge, UK, 1998).
- [12] H. Fujikawa and M. Matsushita, *J. Phys. Soc. Jpn.* **58**, 3875 (1989).
- [13] T. Vicsek, M. Cserző, and V. K. Horváth, *Physica A* **167**, 315 (1990).
- [14] J. I. Wakita, H. Itoh, T. Matsuyama, and M. Matsushita, *J. Phys. Soc. Jpn.* **66**, 67 (1997).
- [15] M. Matsushita, J. Wakita, H. Itoh, I. Ràfols, T. Matsuyama, H. Sakaguchi, and M. Mimura, *Physica A* **249**, 517 (1998).
- [16] M. Nicoli, M. Castro, and R. Cuerno, *J. Stat. Mech.: Theor. Exp.* **2009**, P02036 (2009).
- [17] C. D. Nadell, K. R. Foster, and J. B. Xavier, *PLoS Comp. Biol.* **6**, e1000716 (2010).
- [18] S. Mitri, J. B. Xavier, and K. R. Foster, *Proc. Natl. Acad. U.S.A.* **108**, 10839 (2011).
- [19] C. D. Nadell, V. Bucci, K. Drescher, S. A. Levin, B. L. Bassler, and J. B. Xavier, *Proc. Roy. Soc. B* **280**, 20122770 (2013).
- [20] J. W. Costerton, Z. Lewandowski, D. E. Caldwell, D. R. Korber, and H. M. Lappin-Scott, *Ann. Rev. Microbiol.* **49**, 711 (1995).
- [21] J. N. Wilking, T. E. Angelini, A. Seminara, M. P. Brenner, and D. A. Weitz, *MRS Bulletin* **36**, 385 (2011).
- [22] M. Eden, in *Proceedings of the 4th. Berkeley Symposium on Mathematical Statistics and Probability*, Vol. 4, edited by J. Neyman (U. California Press, Berkeley, 1961) pp. 223–239.
- [23] M. Kardar, G. Parisi, and Y.-C. Zhang, *Phys. Rev. Lett.* **56**, 889 (1986).
- [24] S. G. Alves, T. J. Oliveira, and S. C. Ferreira, *EPL* **96**, 48003 (2011).
- [25] K. A. Takeuchi, *J. Stat. Mech.: Theor. Exp.* **2012**, P05007 (2012).
- [26] T. Kriecherbauer and J. Krug, *J. Phys. A: Math. Theor.* **43**, 403001 (2010).
- [27] I. Corwin, *Rand. Mat.: Theor. Appl.* **01**, 1130001 (2012).
- [28] T. Halpin-Healy and K. A. Takeuchi, *J. Stat. Phys.* **160**, 794 (2015).
- [29] H. Van Beijeren, *Phys. Rev. Lett.* **108**, 180601 (2012).
- [30] C. B. Mendl and H. Spohn, *Phys. Rev. Lett.* **111**, 230601 (2013).
- [31] M. Kulkarni and A. Lamacraft, *Phys. Rev. A* **88**, 021603(R) (2013).
- [32] M. Arzamasovs, F. Bovo, and D. M. Gangardt, *Phys. Rev. Lett.* **112**, 170602 (2014).
- [33] S. Nesic, R. Cuerno, and E. Moro, *Phys. Rev. Lett.* **113**, 180602 (2014).
- [34] M. Prähofer and H. Spohn, *J. Stat. Phys.* **108**, 1071 (2002).
- [35] I. Corwin, J. Quastel, and D. Remenik, *Comm. Math. Phys.* **317**, 347 (2013).
- [36] M. Mimura, H. Sakaguchi, and M. Matsushita, *Physica A* **282**, 283 (2000).
- [37] J. Dockery and I. Klapper, *SIAM J. Appl. Math.* **62**, 853 (2002).
- [38] C. Giverso, M. Verani, and P. Ciarletta, *J. Roy. Soc. Interface* **12**, 20141290 (2015).
- [39] C. Giverso, M. Verani, and P. Ciarletta, *Biomech. Model. Mechanobiol.* **15**, 643 (2016).
- [40] F. D. C. Farrell, O. Hallatschek, D. Marenduzzo, and B. Walclaw, *Phys. Rev. Lett.* **111**, 168101 (2013).
- [41] I. Ràfols, *Formation of concentric rings in bacterial colonies*, Master's thesis, Chuo University (1998).
- [42] M. Castro, R. Cuerno, A. Sánchez, and F. Domínguez-Adame, *Phys. Rev. E* **62**, 161 (2000).
- [43] P. J. Yunker, M. A. Lohr, T. Still, A. Borodin, D. J. Durian, and A. G. Yodh, *Phys. Rev. Lett.* **110**, 035501 (2013).
- [44] M. Nicoli, R. Cuerno, and M. Castro, *Phys. Rev. Lett.* **111**, 209601 (2013).
- [45] P. J. Yunker, M. A. Lohr, T. Still, A. Borodin, D. J. Durian, and A. G. Yodh, *Phys. Rev. Lett.* **111**, 209602 (2013).
- [46] See Supplemental Material at XXX for details on our analysis of front profiles and on our continuum model.
- [47] K. A. Takeuchi and M. Sano, *Phys. Rev. Lett.* **104**, 230601 (2010).
- [48] M. Huergo, M. Pasquale, P. González, A. Bolzán, and A. Arvia, *Phys. Rev. E* **84**, 021917 (2011).
- [49] S. N. Santalla, J. Rodríguez-Laguna, and R. Cuerno, *Phys. Rev. E* **89**, 010401(R) (2014).
- [50] J. M. Pastor and M. A. Rubio, *Phys. Rev. Lett.* **76**, 1848 (1996).
- [51] S. Huo and W. Schwarzacher, *Phys. Rev. Lett.* **86**, 256 (2001).
- [52] F. Ojeda, R. Cuerno, R. Salvarezza, and L. Vázquez, *Phys. Rev. Lett.* **84**, 3125 (2000).
- [53] Y. P. Zhao, J. B. Fortin, G. Bonvallet, G. C. Wang, and T. M. Lu, *Phys. Rev. Lett.* **85**, 3229 (2000).
- [54] M. Castro, R. Cuerno, M. Nicoli, L. Vázquez, and J. G. Buijnsters, *New J. Phys.* **14**, 103039 (2012).
- [55] G. S. Bales, R. Bruinsma, E. A. Eklund, R. P. U. Karunasiri, J. Rudnick, and A. Zangwill, *Science* **249**, 4966 (1990).
- [56] M. L. Frankel and G. I. Sivashinsky, *Phys. Rev. E* **52**, 6154 (1995).
- [57] S. I. Blinnikov and P. V. Sasorov, *Phys. Rev. E* **53**, 4827 (1996).
- [58] J. Rodríguez-Laguna, S. N. Santalla, and R. Cuerno, *J. Stat. Mech.: Theory Exp.* **2011**, P05032 (2011).
- [59] M. Nicoli, R. Cuerno, and M. Castro, *Phys. Rev. Lett.* **102**, 256102 (2009).
- [60] J. Krug, *Adv. Phys.* **46**, 139 (1997).
- [61] M. A. C. Huergo, N. E. Muzzio, M. A. Pasquale, P. H. P. González, A. E. Bolzán, and A. J. Arvia, *Phys. Rev. E* **90**, 022706 (2014).
- [62] N. E. Muzzio, M. A. Pasquale, M. A. C. Huergo, A. E. Bolzán, P. H. González, and A. J. Arvia, *J. Biol. Phys.* **42**, 477 (2016).
- [63] J. M. López and H. J. Jensen, *Phys. Rev. E* **65**, 21903 (2002).
- [64] O. Hallatschek, P. Hersen, S. Ramanathan, and D. R. Nelson, *Proc. Natl. Acad. U.S.A.* **104**, 19926 (2007).
- [65] J. T. Kuhr, M. Leisner, and E. Frey, *New J. Phys.* **13**, 113013 (2011).
- [66] M. Reiter, S. Rulands, and E. Frey, *Phys. Rev. Lett.* **112**, 148103 (2014).

Supplemental material for

“Non-universality of front fluctuations for compact colonies of non-motile bacteria”

Silvia N. Santalla, Javier Rodríguez-Laguna, José P. Abad, Irma Marín, María del Mar Espinosa, Javier Muñoz-García, Luis Vázquez, and Rodolfo Cuerno

1 Extraction of front profiles

In this Section we provide details of the protocol we have followed in order to extract the position of the fronts of the bacterial colonies from the photographs taken. The analysis was semi-automatic. An algorithm was developed, which works in the majority of the cases without supervision. The images were digitized and subject to a contrast filter in order to highlight the interface. The resulting image can be regarded as a matrix with 1 in the inside of the colony and 0 outside. Then, a discretized continuous curve was obtained as follows. First, the geometric center of the colony bulk was estimated. Then we obtained the intensity curve along rays emanating from that point for different angles, $I_\theta(r)$. For each angle θ , we obtained the distance $r(\theta)$ from the center, such that a certain threshold value of the total intensity was found below it. In other terms,

$$\int_0^{r(\theta)} dr I_\theta(r) = \mu \int_0^\infty dr I_\theta(r), \quad (1)$$

where μ is the threshold parameter. In our case, $\mu = 0.99$ was employed, i.e., the radius $r(\theta)$ is defined as the first percentile of the intensity distribution. As an illustration, Fig. 1 shows a set of experimental photographs and the corresponding profiles.

2 Global and local roughness

Once the front profile has been digitized, it is a set of N points on the plane, $\{x_i, y_i\}_{i=1}^N$. This set is employed to obtain the radius of the best fitting circle, using a minimization procedure to find the corresponding center $(x_{\text{CM}}, y_{\text{CM}})$ and radius R . The deviations from the fitting circle provide the *global roughness*,

$$W \equiv \left\langle \frac{1}{N} \sum_{i=1}^N \left(\sqrt{(x_i - x_{\text{CM}})^2 + (y_i - y_{\text{CM}})^2} - R \right)^2 \right\rangle^{1/2}, \quad (2)$$

where brackets denote averages over experimental realizations. Figure 2 of the main text (MT) shows the time evolution of the average radius and roughness for our experimental colonies.

One can also define a local roughness, $w(\ell)$, that evaluates deviations from an average position of the interface within observation windows of size ℓ . We proceed as is customary for systems with an overall circular symmetry [1]: Namely, each point on the front is converted to polar coordinates emanating from the geometric center, $(x_i, y_i) \rightarrow (\theta_i, r_i)$, whereby θ_i (r_i) is considered a new independent (dependent) variable. Given an initial point \vec{r}_0 and a length scale ℓ , we consider the set of points within a circle centered at \vec{r}_0 with radius ℓ . Then, we make a fit to the straight line which minimizes the deviations. The mean-square distance of the front positions to that fitting line provides the *local roughness* $w(\ell)$. In Fig. 3 of the MT we show the local roughness as a function of length-scale ℓ for different times, as obtained in our experiments with *B. subtilis*.

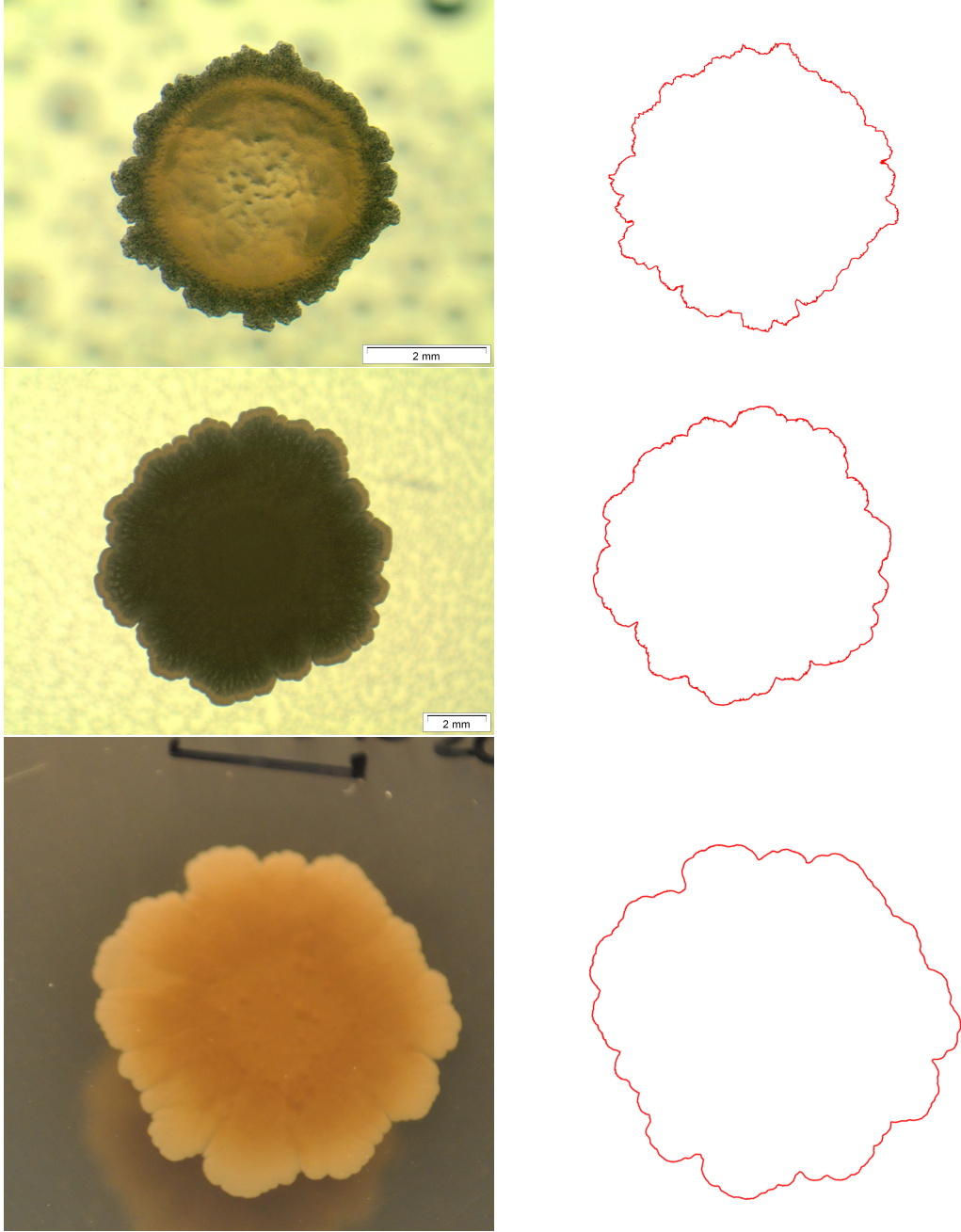


Figure 1: Experimental photographs of the bacterial colonies (left column) and profiles extracted using the procedure described in the text (right column). All these examples corresponds to *B. subtilis* with $C_n = 20$ g/l. The growth times are 19 h, 168 h, and 792 h, top to bottom.

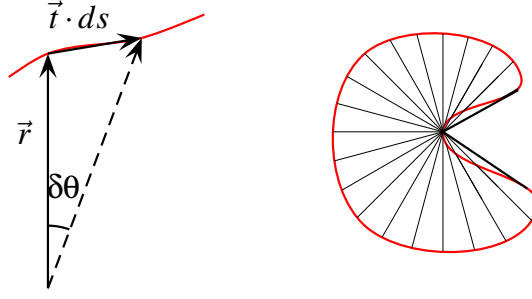


Figure 2: Shadowing angle. Sketch on the left: differential of material angle. The front is the red solid line. Sketch on the right: given the interface shown by the red solid line, the two black straight solid lines delimit the integration region to compute the local shadowing angle at the interface position marked as the center from which all the auxiliary thin solid lines emanate.

3 Phenomenological model

In order to develop a theoretical model for the motion of the boundary of the bacterial colony, we make the following assumptions:

1. The bacterial colony is a two-dimensional object.
2. The dynamics of the colony can be restricted to that of its interface, which can be modeled by a continuous simple curve.
3. The colony interface tends to minimize its length, i.e., it is endowed with a certain surface tension.
4. The nutrient distribution and transport to the colony are heterogeneous in time and space, and their contribution to the local motion of the front can be modeled as an average deterministic term plus fluctuations. For simplicity, the latter are assumed to be uncorrelated in time and space.
5. Nutrients diffuse outside the bacterial colony and inside it, down to a depth of value δ . We will assume that δ can be neglected, so that nutrient transport selectively enhances growth at protuberances as compared to cavities.

3.1 Shadowing angle

A simple implementation of point 5 above is to consider that the nutrient concentration is a monotonous function of *the angle under which a given point at the interface sees the exterior world*. Points inside cavities get less nutrient than those at local protuberances. As frequently done in the context of diffusion-limited growth, intuitively one may make an analogy [1] to an ensemble of grass leaves which are striving to collect sunlight: taller leaves cast shadows on shorter ones, hindering growth of the latter. With this metaphor in mind, the implementation of this effect into our continuum model will be termed a *shadowing term*. The concept is illustrated by the sketch on the right of Fig. 2.

Mathematically, the computation of the shadowing angle is performed as follows. Let us define the *material angle* of an object and a point to be the angle under which the object is seen by an observer standing at that point. For a given infinitesimal segment along the interface, starting

at point \vec{r} and with vector $\vec{t} \cdot ds$ (see the sketch on the left of Fig. 2), the differential of material angle is given by

$$\frac{\vec{r} \times \vec{t} \cdot ds}{r^2} \approx \frac{r^2 \sin(d\theta)}{r^2} \approx d\theta. \quad (3)$$

Direct integration of those angles over a closed curve Γ yields the *winding number* of the curve around the given point,

$$W(\vec{r}_0, \Gamma) = \int_{\Gamma} \frac{(\vec{r} - \vec{r}_0) \times \vec{t}}{|\vec{r} - \vec{r}_0|^2} ds. \quad (4)$$

The material angle, on the other hand, can not be computed as an integral of this kind. We need to obtain the range of possible angles. Let $A(\vec{r}, \vec{r}_0)$ be the angle from which \vec{r} is seen from \vec{r}_0 . Then, the material angle from point \vec{r}_0 is given by

$$\Theta_S(\vec{r}_0) = 2\pi - |\text{Range}_{\vec{r} \in \Gamma}(A(\vec{r}, \vec{r}_0))|. \quad (5)$$

i.e. the measure of the range of function $A(\vec{r}, \vec{r}_0)$ when \vec{r} takes values on Γ .

3.2 Continuum model with shadowing

Let us consider a model for interface growth in which, at each interface position, growth proceeds along the local normal direction, with a speed which is proportional to the local shadowing angle. This dynamics is inherently *unstable*: interface points which lag slightly behind will move less and less at later times, so that relative distances between protuberances and cavities are amplified by the dynamics. This corresponds to the physical situation in which an interface point within a cavity gets less nutrients, so that its growth rate stagnates, while protuberances branch out.

In view of the various considerations made in this section, we propose the following equation for the growth of the colony front [Eq. (1) of the MT]:

$$\partial_t \vec{r} = (A_0 + A_1 K(\vec{r}) + A_S \Theta_S(\vec{r}) + A_n \eta) \vec{n}. \quad (6)$$

Here, \vec{r} is an interface point, \vec{n} is the local exterior normal, $K(\vec{r})$ denotes the extrinsic curvature of the interface at that point, $\Theta_S(\vec{r})$ is the local shadowing angle, η is zero-average, Gaussian uncorrelated space-time noise, and A_0 , A_1 , A_S and A_n are parameters which quantify, respectively, the relative strengths of the average growth velocity of a planar front, surface tension, the dependence on the shadowing angle, and fluctuations. Equation (6) is similar to continuum models earlier put forward in the context of growth of thin solid films limited by diffusive transport, see e.g. [2] for a review. Note that, in contrast with many works in that field, Eq. (6) applies to interfaces with an arbitrary geometry, in particular with an average circular shape, and is not affected by small-slope, nor no-overhang approximations. In this sense, the model can be considered a stochastic generalization of a previous equation put forward in the context of combustion fronts [3, 4], for which transport also takes place by diffusion.

Equation (6) is highly nonlinear. In order to simulate this stochastic integro-differential equation, we have proceeded along the lines of [5, 6]: the interface is discretized in an adaptive way, adding and removing points dynamically in order to keep a constant spatial resolution. The normal vector and the local curvature are computed using concepts from discrete geometry. An important element of the simulation is that the interface is always a simple curve, although it can have *overhangs*: self-intersections are removed.

The evaluation of the shadowing angle is the most costly part of the calculation to simulate Eq. (6), since it is a global measurement. We have devised the following algorithm in order to compute the shadowing angle. Given a point P and a segment $P_1 P_2$, we define the angle-interval as the counterclockwise ordered pair $\alpha(P, P_1 P_2) \equiv (\alpha_0, \alpha_1)$ of angles, with respect to the horizontal, under which the segment is viewed from the point. If a segment is extended to a chain $P_1 \cdots P_n$,

we just compute the union of all angle-intervals. The material angle is the measure of the final angle-interval.

In order to assess the type of morphological instability implied by the shadowing term in Eq. (6), we have simulated it numerically by setting to zero all other terms in the equation. We have performed a linear stability analysis of the ensuing model by studying the rate of growth or decay in time for sinusoid-like perturbations of an overall circular shape (not shown). We have verified the expected unstable behavior: the amplitude of a small perturbation grows with a velocity proportional to the wave-number k of the perturbation. In the case of a band geometry with periodic boundary conditions, this means that, according to Eq. (6),

$$\partial_t h_k(t) \simeq |k| h_k(t) + \dots, \quad (7)$$

where $h_k(t)$ is the amplitude of a small sinusoidal perturbation of a flat profile with wave-vector k . This is indeed the well-known behavior of the shadowing term, as elucidated in other diffusion-limited systems [1, 2, 3, 4].

References

- [1] P. Meakin, *Fractals, scaling and growth far from equilibrium* (Cambridge University Press, Cambridge, UK, 1998).
- [2] G. S. Bales, R. Bruinsma, E. A. Eklund, R. P. U. Karunasiri, J. Rudnick, and A. Zangwill, *Science* **249**, 4966 (1990).
- [3] M. L. Frankel and G. I. Sivashinsky, *Phys. Rev. E* **52**, 6154 (1995).
- [4] S. I. Blinnikov and P. V. Sasorov, *Phys. Rev. E* **53**, 4827 (1996).
- [5] J. Rodríguez-Laguna, S. N. Santalla, and R. Cuerno, *J. Stat. Mech.: Theory Exp.* **2011**, P05032 (2011).
- [6] S. N. Santalla, J. Rodríguez-Laguna, and R. Cuerno, *Phys. Rev. E* **89**, 010401(R) (2014).